

# Metallic thin film thickness determination using electron probe microanalysis

C. S. Campos,<sup>1</sup> E. A. Coleoni,<sup>2</sup> J. C. Trincavelli,<sup>2†</sup> J. Kaschny,<sup>1</sup> R. Hubbler,<sup>3</sup> M. R. F. Soares<sup>1</sup> and M. A. Z. Vasconcellos<sup>1\*</sup>

<sup>1</sup> Instituto de Física, Universidade Federal do Rio Grande do Sul (UFRGS), Porto Alegre, Brazil

<sup>2</sup> Facultad de Matemática, Astronomía y Física, Universidad Nacional de Córdoba, Córdoba, Argentina

<sup>3</sup> Instituto de Física, Pontificia Universidade Católica (RS), Porto Alegre, Brazil

Received 6 October 1999; Accepted 13 March 2001

An experimental procedure to determine metallic thin film thicknesses by using electron probe microanalysis (EPMA) is presented. Several monoelemental films of Al, Ti, Cr, Cu, Nb, Mo and Au with different thicknesses, deposited on an Si substrate, were characterized by Rutherford backscattering spectrometry for thickness measurement. Characteristic x-ray intensities were measured for films, substrate and bulk standards. The ratios of these intensities (*k-ratio*), were compared with those obtained from Monte Carlo simulations based on the subroutine package PENELOPE, and good agreement was found. The results from simulation and experiments were added to build calibration curves of *k-ratio* vs thickness for the monoelemental films investigated. A simple analytical function was fitted to these curves and the behavior of its parameters with atomic number was studied. Copyright © 2001 John Wiley & Sons, Ltd.

## INTRODUCTION

The study of nanostructured material or near-surface modified materials (e.g. nitrating, ion implantation) evaluates structural, magnetic and electric properties. It usually requires the knowledge of the thickness and composition of the surface layer. Several techniques can be used to this end, e.g. Rutherford backscattering spectrometry<sup>1</sup> (RBS). In this technique, the material is irradiated with  $\alpha$ -particles with incident energy in the range 0.5–1.5 MeV. These particles interact with the atoms in the material and the backscattered fraction is quantified in number and energy distribution.

With RBS it is possible to determine the atomic mass of sample constituents, the occurrence of impurities and the depth distribution of the atomic species. The possibility of determining thin-film thicknesses is of special interest for this work. However, some difficulties are observed when characterizing thicknesses <20 nm or >500 nm or when differences between atomic numbers in the sample are small (e.g. Al/Si). Electron probe microanalysis (EPMA) was used in this work as a complementary technique to RBS to overcome some of these difficulties.

In EPMA, elements are differentiated through characteristic x-rays. Typical lateral resolutions are around 1  $\mu\text{m}$ , and the technique can be used to determine thicknesses in a wide range from several micrometers down to a few monolayers. The beam electrons interact with the sample by means of elastic and inelastic scattering within the so-called ionization volume. The ionization depth distribution depends on the

incoming energy of the electrons ( $E_0$ ) and average atomic number ( $Z$ ) of the sample.<sup>2</sup> Irradiation of a monolayer thin film deposited on a bulk substrate with fixed  $E_0$  will induce the generation of characteristic x-rays from film and substrate in relative amounts defined by the ionization depth distribution in the interaction volume. By changing the thickness of the film, different relative intensities from film and substrate are generated. These intensities of characteristic x-rays from film and substrate are compared with bulk standards, defining a quantity called the *k-ratio*.

The EPMA characterization of films deposited on a substrate has been studied by several groups,<sup>3–10</sup> following different approaches. Usually a semiempirical analytical function is proposed to predict the film thickness.<sup>3–8</sup> Certain parameters involved in the analytical description are not easy to establish from a pure theoretical basis, and Monte Carlo simulation<sup>9–11</sup> became a powerful tool to assess them. In the present work, an experimental procedure was followed to construct calibration curves relating experimental *k-ratio* to film thickness. This approach is restricted to the particular set of samples considered but could be extended to other film–substrate configurations by performing new measurements. On the other hand, the semiempirical analytical procedures are more general, but involve several approximations, which are not assumed in the method proposed here.

The calibration curves were obtained by measuring EPMA *k-ratios* for several monoelemental films of different thickness; these results were assigned to the corresponding thicknesses determined from RBS measurements. Thickness values obtained from RBS were also used as input parameters for Monte Carlo simulation using the PENELOPE code,<sup>12</sup> in order to compare the results from experiment and simulation.

\*Correspondence to: M. A. Z. Vasconcellos, Instituto de Física, Universidade Federal do Rio Grande do Sul (UFRGS), Porto Alegre, Brazil.

†Consejo Nacional de Investigaciones Científicas y Técnicas de la República Argentina.

The simulation results were added to extend the thickness range of the calibration curves for the mono-elemental films investigated. A function was fitted to these curves and the behavior of its parameters with atomic number was studied.

## EXPERIMENTAL

Mono-elemental films were sputter-deposited on Si(111) substrates using a Balzers BAS-450 deposition system. Elements used for measurements of characteristic  $K\alpha$  x-rays were Al, Ti, Cr and Cu and elements used for  $L\alpha$  measurements were Cu, Nb, Mo and Au. All films were deposited under the same control parameters of the equipment. Different thicknesses were obtained by varying the sputtering times. Table 1 gives the sputtering times for the set of films under investigation. Au films were vapor deposited over an Si(111) substrate.

Results from RBS were acquired from a Tandemron Accelerator from High Voltage Engineering with 3 MeV at the Laboratório de Implantação de Ions at the Universidade Federal do Rio Grande do Sul, Brazil. Ion beams of  $\alpha$ -particles with energies of 760 keV and 1 MeV were used. The system resolution was 14 keV and beam current was low enough to avoid experimental artifacts such as pile-up or sample heating.

EPMA measurements were performed in a CAMECA SX-50 at the Laboratório de Microsonda Eletrônica of the Universidade Federal do Rio Grande do Sul. Characteristic x-ray intensities were determined by wavelength-dispersive spectrometry. The crystals used were TAP (Al  $K\alpha$ , Si  $K\alpha$ , Cu  $L\alpha$ , Nb  $L\alpha$ ), PET (Ti  $K\alpha$ , Cr  $K\alpha$ , Nb  $L\alpha$ , Mo  $L\alpha$ ), and LIF (Cu  $K\alpha$ , Au  $L\alpha$ ). The electron beam acceleration voltage was varied between 10 and 20 keV in steps of 1 or 2 keV. The beam current was set 10 nA and the beam diameter was 1  $\mu$ m. The acquisition time was 30 s in each analyzed position for the signals from film, substrate and corresponding standards.

## RESULTS

### Rutherford backscattering spectrometry

Figure 1 shows typical RBS spectra for Cu thin films with varying thickness. Energy edges are indicated for  $\alpha$ -particles backscattered from collisions with (i) atoms of copper located

at the surface (Cu-edge), (ii) atoms of copper located at the interface (Cu/Si-edge) and (iii) atoms of silicon at the same interface (Si-edge). Film thicknesses  $\Delta x_i$  corresponding to different deposition times are also indicated. The energy width  $\Delta E$ , corresponding to the difference between the Cu-edge and the Cu/Si-edge, is proportional to film thickness. Signal from a copper bulk sample is also shown. The inset shows the geometry of the experiment schematically.

The first step to determine film thickness from the RBS spectrum is to obtain the energy width  $\Delta E$ . This quantity can be determined by fitting the spectral region related to the film using the function

$$Y = A \operatorname{erf}\left(\frac{X - C + D}{B + S}\right) - \operatorname{erf}\left(\frac{X - C}{B}\right) \exp^{-\left(\frac{X - C}{T}\right)} \quad (1)$$

where  $A$  is a scale factor proportional to acquisition time,  $B$  is the width of the error function at the Cu-edge,  $C$  accounts for the energy position of the Cu-edge,  $D$  is  $\Delta E$ ,  $S$  takes into account the signal width at the Cu/Si interface due to the 'straggling' of  $\alpha$ -particles at this position,  $X$  is the  $\alpha$ -particle energy (keV),  $Y$  is the number of counts and  $T$  is a free parameter.

The first error function fits the signal from the Cu/Si interface and the second the signal from the surface, and the exponential factor modulates the signal amplitude due to the increase in the cross-section of the  $\alpha$ -particle with decreasing energy.

The next step is to calculate the integrals

$$\begin{aligned} \frac{x}{\cos \Theta_1} &= - \int_{E_0}^E \left(\frac{dE}{dx}\right)^{-1} dE = - \int_{E_0}^E \sum_{n=0}^E A_n E^n dE \\ &= - \sum_{m=0}^E \frac{A_m E^{(m+1)}}{m+1} \Bigg|_{E_0}^E \end{aligned} \quad (2)$$

$$\begin{aligned} \frac{x}{\cos \Theta_2} &= - \int_{KE}^{E_1} \left(\frac{dE}{dx}\right)^{-1} dE = - \int_{KE}^{E_1} \sum_{n=0}^{E_1} A_n E^n dE \\ &= - \sum_{n=0}^{E_1} \frac{A_n E^{(n+1)}}{n+1} \Bigg|_{KE}^{E_1} \end{aligned} \quad (3)$$

From Eqns (2) and (3),

$$\cos \Theta_2 F(KE, E_1) - \cos \Theta_1 F(E_0, E) = 0 \quad (4)$$

**Table 1.** Sputtering deposition time for the films and the thickness determined by RBS

| Deposition time (min) | Thickness (nm) |
|-----------------------|----------------|-----------------------|----------------|-----------------------|----------------|-----------------------|----------------|
| Cu                    |                | Ti                    |                | Cr                    |                | Nb                    |                |
| 1                     | 128.0          | 1                     | 34.6           | 1                     | 57.5           | 1                     | 39.4           |
| 2                     | 280.4          | 2                     | 69.5           | 2                     | 112.9          | 2                     | 78.8           |
| 3                     | 437.2          | 3                     | 91.6           | 3                     | 164.8          | 3                     | 123.1          |
| –                     | –              | 4                     | 142.2          | 4                     | 217.2          | 4                     | 160.0          |
| Mo                    |                | Al                    |                | Au                    |                |                       |                |
| 1                     | 59.6           | 1                     | 83.9           | 0.5                   | 46.7           |                       |                |
| 2                     | 119.7          | 2                     | 187.1          | 1.5                   | 101.7          |                       |                |
| 3                     | 174.2          | 3                     | 265.2          | 2.5                   | 145.6          |                       |                |
| –                     | –              | 4                     | 401.5          | –                     | –              |                       |                |

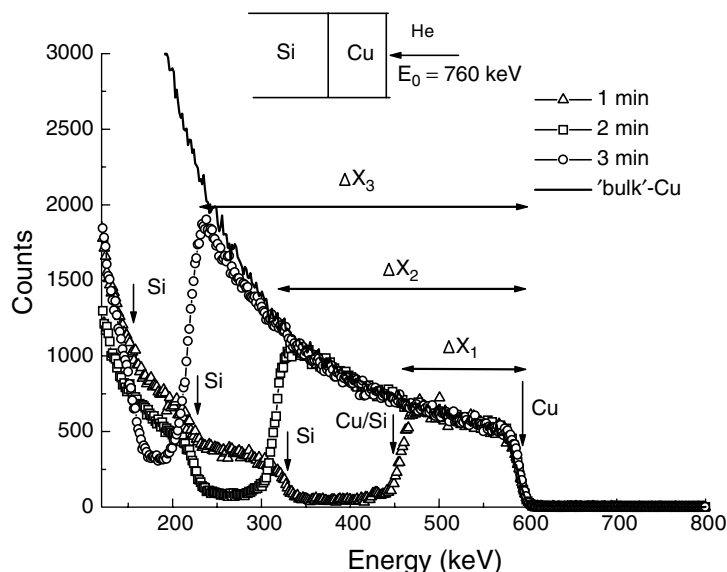


**Figure 1.** Rutherford backscattering spectra from monoelemental films of Cu, sputter deposited on Si substrate for different times ( $\Delta$ , 1 min;  $\square$ , 2 min;  $\circ$ , 3 min; solid line, bulk Cu)  $\Delta x_i$  represents the film thickness. Vertical arrows indicate the edge positions at the film surface, film/substrate interface and bulk material.

where

$$F(KE, E_1) = \sum_{n=0} \left( \frac{A_n E^{(n+1)}}{n+1} \right)_{KE}^{E_1} \text{ and}$$

$$F(E_0, E) = \sum_{n=0} \left( \frac{A_n E^{(n+1)}}{n+1} \right)_{E_0}^E \quad (5)$$

The energy loss ( $dE/dx$ ) is determined by fitting a tenth-order polynomial with data generated from the simulation software SR.EXE which is part of the software package TRIM, version 1992, where values for stopping power and range of  $\alpha$ -particles as a function of energy are calculated by using the ZBL procedure.<sup>13</sup> The angles  $\Theta_1$  and  $\Theta_2$  are determined from the experimental geometry.  $\Theta_1$  is the angle between ion beam and the normal to the surface and  $\Theta_2$  is the angle between the detector position and the normal to the surface. In the present work they were set to 0 and 160°, respectively.  $E_0$  is the energy of the incident particles.  $K$  is the kinematic factor.  $KE_0$  is the energy of the  $\alpha$ -particles backscattered from the surface of the film.  $E$  is the energy of the  $\alpha$ -particles immediately before scattering at the film/substrate interface and is unknown.  $KE$  is the energy of the  $\alpha$ -particles immediately after scattering at the film/substrate interface and  $E_1$  is the energy of the particles scattered from the interface when emerging from the film surface. The iterative numerical procedure presented in this section was developed by one of the authors (J. Kaschny) to determine  $E$ , and using Eqn (2) or (3), determine the thickness  $x$ . Table 1 shows all film thickness values calculated by means of the procedure described above.

### Electron probe microanalysis

Films were characterized by EPMA through the parameter  $k$ -ratio, defined as the ratio between the characteristic x-ray intensity emerging from the film and the intensity measured from a bulk standard of the same (pure) composition. A similar ratio is defined for the signal from the substrate. The

nomenclature for  $k$ -ratios from film and substrate is

$$K_F = \frac{I_F}{I_{BF}}$$

for the film and

$$K_S = \frac{I_S}{I_{BS}}$$

for the substrate, where  $I_F$  is the intensity of characteristic x-rays emerging from the film,  $I_{BF}$  is the intensity measured in a bulk standard with the same monoelemental composition as the film,  $I_S$  is the intensity from the substrate material and  $I_{BS}$  is the intensity measured in a bulk standard with the same monoelemental composition as the substrate.

Figure 2 shows the typical behavior of the  $k$ -ratio as a function of electron beam energy for the case of Al/Si and Cu/Si films. This kind of result allows one to determine the best option of the energy value to be used when constructing calibration curves for a specific range of thickness. For the nominal thickness chosen for Al films, the difference between values of the  $k$ -ratio is higher for decreasing values of  $E_0$ . The sensitivity for differentiating films with close thickness values will therefore be greater for low  $E_0$  values.

### Monte Carlo simulation technique

Monte Carlo simulation results presented in this work were obtained using the subroutine package PENELOPE (Penetration and ENERGY LOSS of Positrons and Electrons)<sup>12</sup> and the simulation code PENSPT<sup>14</sup> to generate characteristic x-ray spectra. Electron interactions are divided into two contributions, elastic and inelastic scattering. The realistic cross-sections used to describe them produced results successfully in a wide range of applications with the energy of electrons and photons impinging materials varying from 1 GeV down to 100 eV.<sup>15-17</sup> In addition, some results produced by PENELOPE were compared with a more rigorous (and slow) simulation code.<sup>16</sup> In the present work, the simulation

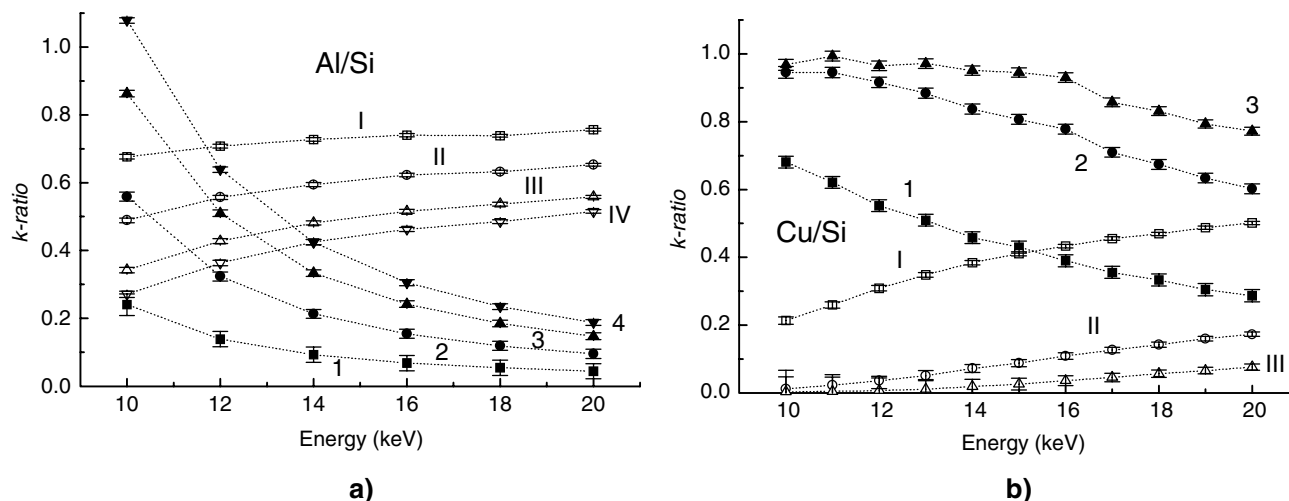


**Figure 2.** Experimental results for  $k$ -ratio versus electron beam energy for (a) Al and (b) Cu films deposited on Si substrate. Numbers 1, 2, 3 and 4 are deposition times in minutes for the film and indicate the measured signal from the films. Numbers I, II, III and IV indicate the corresponding signal measured from the Si substrate.

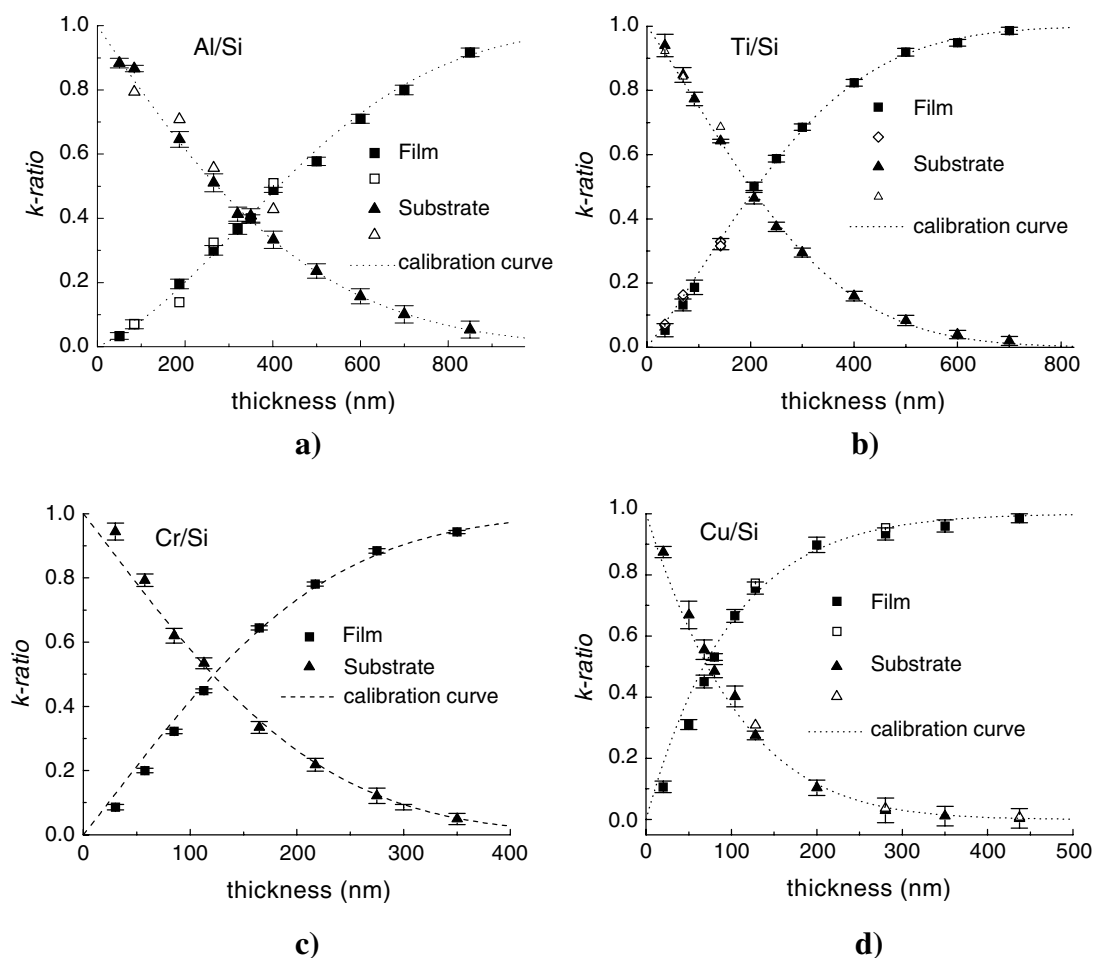


**Figure 3.** Plots of  $k$ -ratio vs thickness with results from experiment and MC simulations for (a) Al/Si, (b) Ti/Si, (c) Cr/Si (only simulations) and (d) Cu/Si films. Open symbols are related to experimental results and solid symbols represent results from Monte Carlo simulations for film and substrate material. The calibration curve, represented by dots, was fitted using Eqn (6). Electron beam energy was 12 keV for these results.

results consist of the spectral distribution of characteristic and bremsstrahlung photons emitted by the sample.

The geometry of monoelemental films of Al, Ti, Cr and Cu over an Si substrate was simulated at an energy of 12 keV.

The same energy was used to simulate bulk standards for the same elements.

Figure 3 shows experimental and simulated EPMA results for  $k$ -ratio vs thickness determined from RBS. For

comparison between experiment and simulation, some of the thickness values used for the simulation were those determined from RBS. Because of the good agreement observed, several simulations were performed to extend the thickness range of these curves. Cr/Si films were not characterized by EPMA and only results from simulation are presented in the figure.

**DISCUSSION**

The combined use of experimental and simulated data allowed us to obtain calibration curves in a wide thickness range. For practical use of these results, a simple analytical function was fitted according to a general behaviour proposed previously:<sup>11</sup>

$$K_F = 1 - e^{-(Ax+Bx^2)} \text{ and } K_S = e^{-(Cx+Dx^2)} \quad (6)$$

where  $K_F$  and  $K_S$  are the  $k$ -ratio for film and substrate, respectively, and  $A$ ,  $B$ ,  $C$  and  $D$  are free parameters

adjusted from the experimental results. Figure 4(a) shows the simulated  $k$ -ratio values for Al, Ti, Cr and Cu films at 12 keV incident energy as a function of film thickness. The corresponding fitting curves given by Eqn (6) are also plotted. As can be seen, the curves have a strong dependence on film atomic number. In order to analyze the results independently of film density, the variable  $x$  in Eqn (6) is changed to  $\rho x$  and the results from the fitting curves are shown in Fig. 4(b). The dependence of film signal on atomic number remains evident. On the other hand, the signal from the substrate exhibits a more clustered behavior. These trends are quantitatively accounted for by the parameters  $A$ ,  $B$ ,  $C$  and  $D$  in Eqn (6). The variation of these parameters with atomic number is depicted in Fig. 5. Table 2 presents the values of linear and quadratic fitting parameters to obtain  $K_F$  and  $K_S$ , at  $K\alpha$  x-ray lines, at 12 keV electron beam energy.

Equation (6) resembles attenuation curves, hence the parameter  $A$  can be associated with the attenuation of

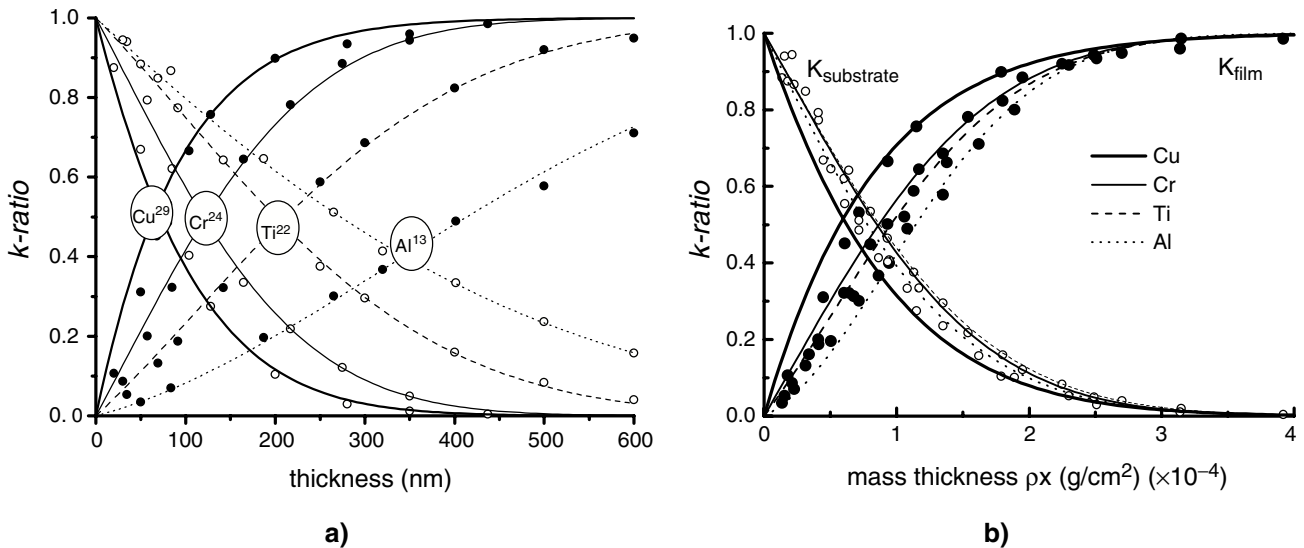


**Figure 4.** (a)  $k$ -ratio vs thickness and (b)  $k$ -ratio vs mass thickness with results from MC simulations for Al/Si, Ti/Si, Cr/Si and Cu/Si films and substrate. The calibration curves were fitted using Eqn (6). Electron beam energy was 12 keV for these simulations.

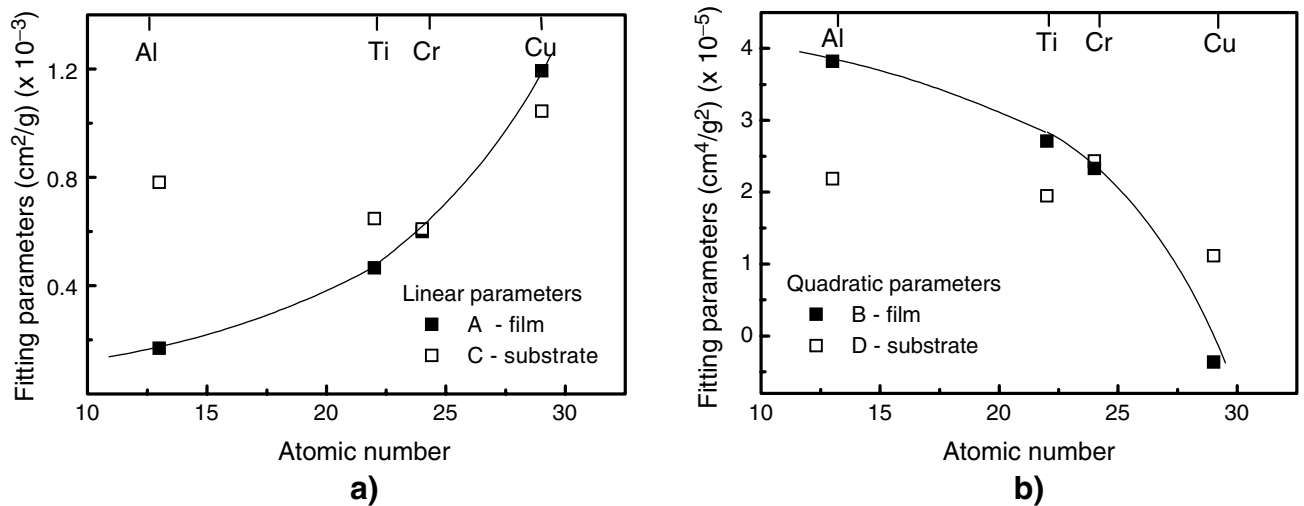


**Figure 5.** Plots of (a) linear and (b) quadratic fitting parameters against the atomic number from the films characterized through  $K\alpha$  x-ray lines and using Eqn (6). Electron beam energy was 12 keV.

**Table 2.** Values of linear and quadratic fitting parameters to obtain  $K_F$  and  $K_S$ , for  $K\alpha$  x-ray lines using Eqn (6) with  $x$  changed to  $\rho x$  (electron beam energy was 12 keV)

| Element         | $A$<br>( $\text{cm}^2 \text{g}^{-1}$ ) | $B$<br>( $\text{cm}^4 \text{g}^{-2}$ ) | $C$<br>( $\text{cm}^2 \text{g}^{-1}$ ) | $D$<br>( $\text{cm}^4 \text{g}^{-2}$ ) |
|-----------------|--|--|--|--|
| Al ( $Z = 13$ ) | 1694.6                                 | 38222021.8                             | 7183.9                                 | 21896523.6                             |
| Ti ( $Z = 22$ ) | 4662.4                                 | 27119260.4                             | 6023.0                                 | 22179413.6                             |
| Cr ( $Z = 24$ ) | 5997.7                                 | 23300101.1                             | 6088.7                                 | 24327400.1                             |
| Cu ( $Z = 29$ ) | 11936.9                                | -3631304.5                             | 10441.0                                | 11153469.6                             |

electrons and photons in the films whereas electron backscattering and other effects are accounted for by the parameter  $B$ . These phenomena are manifested in the values of  $k$ -ratio through a balance between the linear and quadratic terms in Eqn (6). For a given incident beam energy and film mass thickness, an increase in film atomic number will result

in more efficient stopping of electrons, and therefore more ionizations will occur within the film. This in turn results in a smaller number of ionizations originated by electrons backscattered from the substrate. This behavior is observed in Eqn (6) by the dominance of the linear term in the exponential function. For increasing penetration depth inside the film, the electron beam energy decreases and the elastic scattering is more probable, and the quadratic term in Eqn (6) is dominant in this case. Figure 6 shows the mass-depth functional behavior of the linear and quadratic terms ( $A$  and  $B$ ) for Ti and Cu  $K\alpha$  lines. A crossover between linear and quadratic terms is observed to occur at a higher depth with increasing film atomic number. Parameters  $C$  and  $D$ , related to the substrate signal, show the same trend, although not as evident.

When considering films with characteristic  $L\alpha$  x-rays, the opposite behavior is observed for the linear and quadratic coefficients in Eqn (6). Figure 7 shows the behavior of linear

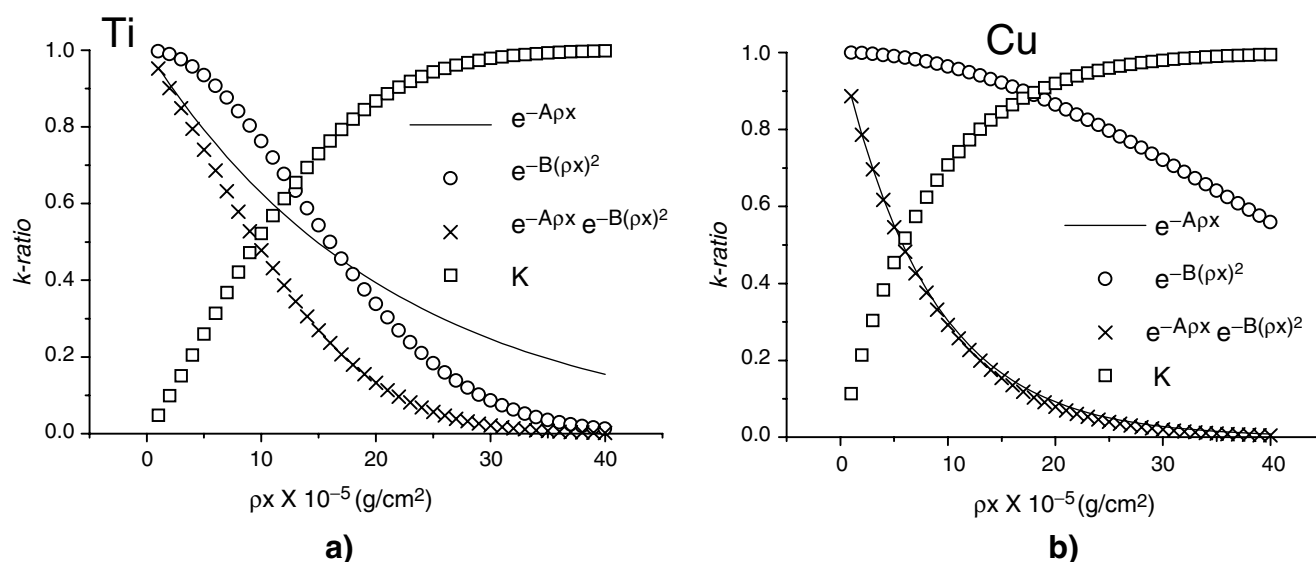


**Figure 6.** Functional behavior of the linear term and quadratic term in the exponential, and  $k$ -ratio of Eqn (6) for (a) Ti/Si and (b) Cu/Si films.

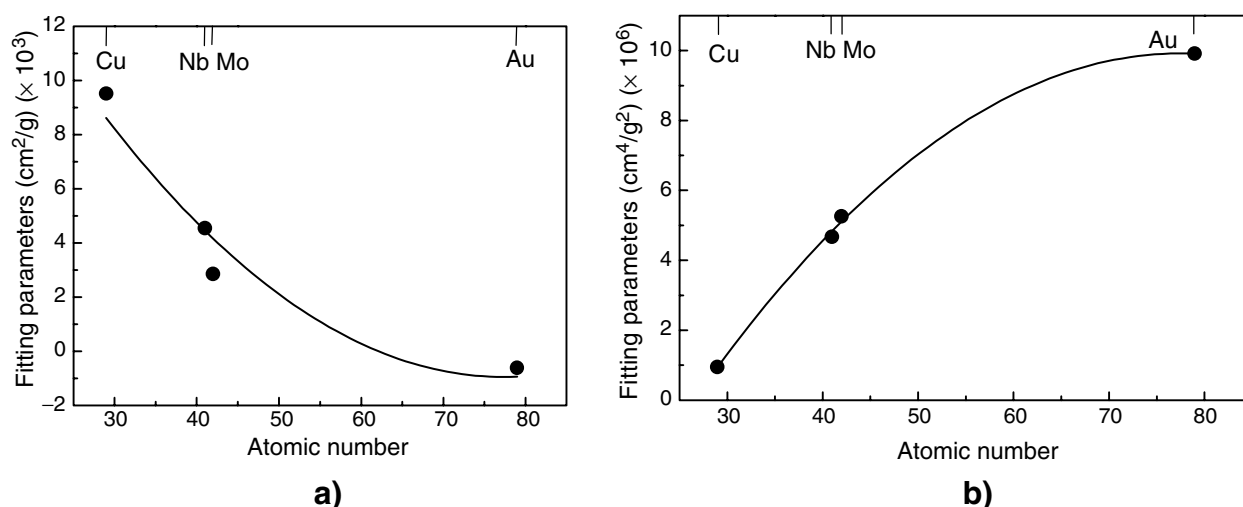


**Figure 7.** Plots of (a) linear and (b) quadratic fitting parameters against the atomic number from the films characterized through  $L\alpha$  x-ray lines and using Eqn (6). Electron beam energy was 12 keV.

**Table 3.** Values of linear and quadratic fitting parameters to obtain  $K_F$ , for  $L\alpha$  x-ray lines using Eqn (6) with  $x$  changed to  $\rho x$  (electron beam energy was 12 keV)

| Element         | $A(\text{cm}^2 \text{g}^{-1})$ | $B(\text{cm}^4 \text{g}^{-2})$ |
|-----------------|--------------------------------|--------------------------------|
| Cu ( $Z = 29$ ) | 9510.2                         | 953403.87                      |
| Nb ( $Z = 41$ ) | 4550.28                        | $4.67588 \times 10^6$          |
| Mo ( $Z = 42$ ) | 2856.8                         | $5.26282 \times 10^6$          |
| Au ( $Z = 79$ ) | 613.68                         | $9.91468 \times 10^6$          |

and quadratic parameters as a function of atomic number of films with elements characterized using  $L\alpha$  lines (Cu, Nb, Mo and Au films). The solid lines are the fitting curves using the function for  $K_F$  given in Eqn (6). The linear parameter decreases and the quadratic parameter increases with increasing atomic number (Table 3). The attenuation term dominates the backscattering term for lower mass depths. Further studies are in progress to increase the database for elements characterized using  $L\alpha$  lines in order to investigate the difference in the behavior of the linear and quadratic terms.

A comparison of the experimental  $k$ -ratios given by Bastin *et al.*<sup>5</sup> and the corresponding values obtained from Eqn (6) for two different thicknesses of Ti films on an Si substrate was performed. For a thickness of  $23.63 \mu\text{g cm}^{-2}$  the corresponding measured  $k$ -ratio was 0.10 against 0.12 from Eqn (6). For the other film with thickness  $4.64 \mu\text{g cm}^{-2}$  the measured  $k$ -ratio was 0.014 against 0.022 from Eqn (6). The reasonable agreement for the first thickness was obtained in spite of the differences in the methods used in each work to determine thicknesses (RBS vs sheet resistivity). Uncertainties related to these methods can encompass the differences observed in  $k$ -ratios. For the second thickness (around 10 nm), the discrepancy is due to the extrapolation of Eqn (6) out from its range of validity, since Ti film thicknesses used in this work to obtain the parameters  $A$  and  $B$  in Eqn (6) were between 34 and 142 nm. It should be emphasized that this kind of comparison is very difficult to perform, since several experimental conditions must be the same in both sets of data to be compared (take-off angle, incidence energy, film–substrate configuration, etc.).

## CONCLUSIONS

EPMA was used in addition to RBS in order to construct calibration curves to determine thicknesses for a set of monoelemental films by measuring characteristic  $K\alpha$  and  $L\alpha$  x-ray intensities.

Experimental results for  $k$ -ratio values were compared with Monte Carlo simulations using the PENELOPE code and good agreement was found. This corroborates the models for electron–matter/photon–matter interactions

assumed in the code when applied to thin-film geometry. This comparison was restricted to  $K\alpha$  lines, since the simulation of characteristic  $L\alpha$  lines was not available in PENELOPE.

Combined data from both experiment and simulation were used to extend the results to a wide range of film thicknesses. A second-order exponential function was used to fit the data and its parameters were evaluated in terms of film atomic number. The role of these parameters was assumed to correspond to a competing effect of electron attenuation and elastic recoil.

By performing fast measurements (a few minutes), the intensity of x-ray emission from film, substrate and bulk standards from the same materials can be performed to obtain the  $k$ -ratios. These  $k$ -ratios values and the values of the linear and quadratic parameters can be used in the exponential function to obtain the mass thickness of a monoelemental film.

## Acknowledgments

Jorge Trincavelli acknowledges financial support from the Consejo Nacional de Investigaciones Científicas y Técnicas de la República Argentina and M. A. Z. Vasconcellos from the Conselho Nacional de Desenvolvimento Científico e Tecnológico—CNPq.

## REFERENCES

1. Chu WK, Mayer JW, Nicolet MA. *Backscattering Spectrometry*. Academic Press: New York, 1978.
2. Goldstein JI, Newbury DE, Echlin P, Joy DC, Fiori CE, Lifshin E. *Scanning Electron Microscopy and X-Ray Microanalysis*. Plenum Press: New York, 1981.
3. Yakowitz H, Newbury DE. *SEM* 1976; **1**: 151.
4. Pouchou JL, Pichoir F. In *Electron Probe Quantitation*, Heinrich KFJ, Newbury DE (eds). Plenum Press: New York, 1991; 31.
5. Bastin GF, Dijkstra JM, Heijligers HJM, Klepper D. In *Proceedings of EMAS'98 3rd Regional Workshop, Barcelona*. 1998; 25–55.
6. Brown JD, Packwood RH. *Appl. Surf. Sci.* 1986; **26**: 294.
7. Hunger HJ. *Scanning* 1988; **10**: 65.
8. August HJ, Wernish J. *Scanning* 1987; **9**: 145.
9. Kyser DF, Murata K. *IBM J. Res. Dev.* 1974; **18**: 352.
10. Roming AD, Plimpton SJ, Michael JR, Myklebust RL, Newbury DE. *Microbeam Analysis*. San Francisco Press: San Francisco, 1990.
11. Coleoni EA. Doctoral Thesis, Universidad Nacional de Córdoba, 1998.
12. Baró J, Sempau J, Fernández-Varea JM, Salvat F. *Nucl Instrum. Methods B* 1995; **100**: 31.
13. Ziegler JF, Biersack JP, Littmark. *The Stopping and Range of Ions in Solids*. Pergamon Press: New York, 1985.
14. Acosta E, Llovet X, Coleoni E, Riveros J, Salvat F. *J. Appl. Phys.* 1998; **83**: 6038.
15. Llovet X, Riveros J, Salvat F. *Mikrochim. Acta (Suppl.)* 1996; **13**: 409.
16. Acosta E, Coleoni E, Castellano G, Riveros J, Fernández Varea JM, Salvat F. *Scanning Microsc.* 1996; **10**: 625.
17. Llovet X, Merlet C, Salvat F. *Mikrochim. Acta (Suppl.)* 1998; **15**: 155.